



NTNU – Trondheim
Norwegian University of
Science and Technology

Thermal-Hydraulic Analysis of a Pneumatic Resonating Device

Per-Kristian Pedersen

Master of Science in Product Design and Manufacturing

Submission date: June 2012

Supervisor: John Sidders, EPT

Norwegian University of Science and Technology
Department of Energy and Process Engineering

EPT-M-2012-71

MASTER THESIS

for

Per-Kristian Pedersen

Spring 2012

Thermal-Hydraulic Analysis of a Pneumatic Resonating Device

*Termisk-Hydraulisk Analyse av en pneumatisk resonerende Device***Background and objective**

The company Resonator AS is currently developing a gas seal and this will become a new product. Resonator AS have investigated the market for solutions to this problem and have been unable to find a seal that meets their intended specification. The specification for the new seal is that it must be capable of operation with high speed linear motion and at high gas pressure (up to 300 bar). The intended use for this seal is in a resonator hammer drilling system associated with drilling for oil. Analysis conducted on this device has shown that the levels of friction generated by the current sealing technology is likely to cause failure due to excessive temperatures being developed.

The object of this project is to extend the analysis to quantify whether changes to the design and cooling arrangements can produce a satisfactory and stable solution, such that both the seal and associated components are maintained within design operating temperatures. The mathematical models should ideally be validated by experimental data.

The following tasks are to be considered:

1 Literature survey

The student must complete a literature survey on high performance pneumatic seals and in particular establish bounds for friction levels for suitable sealing materials

2 The student should develop numerical methods for combining transient calculations for convection and conduction problems

3 Consider the implications of using the perfect gas law to calculate gas properties given the operational pressure range for the gas.

4 Where possible obtain experimental or manufacturers data for key parameters.

Within 14 days of receiving the written text on the master thesis, the candidate shall submit a research plan for his project to the department.

When the thesis is evaluated, emphasis is put on processing of the results, and that they are presented in tabular and/or graphic form in a clear manner, and that they are analyzed carefully.

The thesis should be formulated as a research report with summary both in English and Norwegian, conclusion, literature references, table of contents etc. During the preparation of the text, the candidate should make an effort to produce a well-structured and easily readable report. In order to ease the evaluation of the thesis, it is important that the cross-references are correct. In the making of the report, strong emphasis should be placed on both a thorough discussion of the results and an orderly presentation.

The candidate is requested to initiate and keep close contact with his/her academic supervisor(s) throughout the working period. The candidate must follow the rules and regulations of NTNU as well as passive directions given by the Department of Energy and Process Engineering.

Risk assessment of the candidate's work shall be carried out according to the department's procedures. The risk assessment must be documented and included as part of the final report. Events related to the candidate's work adversely affecting the health, safety or security, must be documented and included as part of the final report.

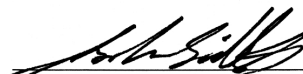
Pursuant to "Regulations concerning the supplementary provisions to the technology study program/Master of Science" at NTNU §20, the Department reserves the permission to utilize all the results and data for teaching and research purposes as well as in future publications.

The final report is to be submitted digitally in DAIM. An executive summary of the thesis including title, student's name, supervisor's name, year, department name, and NTNU's logo and name, shall be submitted to the department as a separate pdf file. Based on an agreement with the supervisor, the final report and other material and documents may be given to the supervisor in digital format.

Department of Energy and Process Engineering, 10. January 2012



Olav Bolland
Department Head



John Sidders
Academic Supervisor

Abstract

Resonator AS is developing a hammer drilling system suitable for oil and geothermal drilling. The nature of the device involves high speed linear motion at high frequencies. As a result of this, the gas springs used in their device are subject to high pressures and temperatures. To prevent pressure leakage from the device, seals are installed.

The seals used in the device are fit for use in a limited range of temperatures and pressures. This pose a challenge since a high amount of heat is generated as a result of the friction between the seal and and the gas spring walls.

The main objective of this thesis has been to develop a model to investigate the effects of the frictional heat. Control volume techniques have been used to model the effects on the gas pressure and temperature. A detailed heat transfer formulation comprising convection and conduction has been developed. To model the conduction it was necessary to derive two-dimensional heat transfer equations for cylindrical coordinates. A MATLAB-code has been written in order to simulate the behavior of the system.

Test results have been compared with the simulations to validate the model. The comparison showed that the model described the thermal inertia of the system appropriately. It also showed that the present friction model is not able to describe the friction in a satisfactory manner.

Sammendrag

Resonator AS utvikler et hammerboringssystem egnet for olje- og geotermisk boring. De lineære bevegelsene i systemet skjer med høy hastighet og høy frekvens. Som et resultat av dette er de pneumatiske fjærene i systemet utsatt for høyt trykk og høye temperaturer. For å hindre trykklekkasje fra enheten, er pakninger installert.

Pakningene som brukes har et begrenset driftsområde med tanke på trykk og temperatur. Dette er utfordrende siden store mengder varme genereres som følge av friksjon mellom pakning og sylinder/stempelstag.

Hovedmålet med denne avhandlingen har vært å utvikle en modell for å undersøke hvordan friksjonsvarmen påvirker systemet. Kontrollvolumanalyse er benyttet for å modellere hvordan gassens trykk og temperatur påvirkes. For å oppnå nøyaktige resultater har varmeoverføringen mellom gassen og gassfjærens komponenter blitt viet ekstra oppmerksomhet. For å modellere konduksjonen var det nødvendig å utlede to-dimensjonale varmeligninger for sylindriske koordinater. Modellen har blitt implementert i en MATLAB-kode for å simulere systemets oppførsel.

Testresultatene har blitt sammenlignet med simuleringer for å validere modellen. Sammenligningen viste at modellen beskriver systemets termisk treghet tilfredsstillende. Den nåværende friksjonsmodellen viste seg imidlertid å ikke holde mål med tanke på å beskrive friksjonen.

Preface

This master thesis has been written at the Waterpower Laboratory, Department of Energy and Process Engineering, at the Norwegian University of Science and Technology during the spring of 2012.

The aim of the thesis has been to develop a dynamic model of a pneumatic spring currently being developed by Resonator AS.

I wish to thank my advisor, Professor John Sidders, for sharing his knowledge and experience with me. I sincerely feel that I have learned a lot. I also wish to thank Pingju Li and the staff at Resonator AS for helpful input while writing the thesis, and for providing me with a challenging and interesting task.

At last I want to pay my gratitude to my fellow students, Lorentz Fjellanger Barstad for advise on the graphical use interface and Simen Vogt-Svendsen for good discussions along the way.

Per-Kristian Pedersen
Trondheim, June 8, 2012

Contents

1	Introduction	1
2	System description	3
3	Modeling	5
3.1	Assumptions and simplifications	5
3.2	Volume and piston velocity	6
3.3	Leakage flow	7
3.4	Enthalpy and Internal energy	8
3.5	Friction	8
3.6	Heat Transfer	10
3.7	Energy equation	11
4	Results and discussion	15
4.1	Case 1	15
4.2	Case 2	22
4.3	Final discussion	22
5	Conclusion	23
6	Further Work	25
A	Ideal versus real gas	29
B	Areas	31
C	Derivation of heat equations	33
C.1	Equation for internal node	33
C.2	Equation for node on the wall on the inside of the cylinder	34
C.3	Equation for nodes on the wall on the outside of the cylinder	35
C.4	Equation for nodes on the bottom/top of the cylinder	36
C.5	Equation for internal corner on the inside of the cylinder	38
C.6	Equation for internal corner on the outside of the cylinder	39
C.7	Equation for external corner on the inside of the cylinder	40
C.8	Equation for external corner on the outside of the cylinder	42
D	The program	43
E	Simulations and tests	45

List of Symbols

Symbols

α	thermal diffusivity, m^2/s
γ	ratio of specific heats
μ_k	kinetic friction coefficient
ν	kinematic viscosity, m^2/s
ω	angular frequency, rad/s
ρ	density, kg/m^3
A	area, m^2
B	piston amplitude, m
c_p	specific heat capacity at constant pressure, J/kgK
e	specific energy, J/kg
f	frequency, Hz ; friction factor
F_f	friction force, N
H	enthalpy, J
h	specific enthalpy, J/kg ; convective heat transfer coefficient, W/m^2K
k	thermal conductivity, W/mK
L	initial length of chambers, m
m	mass, kg
N	normal force, N
Nu	Nusselt number
p	pressure, Pa
Pr	Prandtl number
Q	heat, J
R	gas constant, $J/kg \cdot K$
r	radius, m
Re	Reynolds number
T	temperature, K

t	time, s
U	internal energy, J
u	specific internal energy, J/kg
V	volume, m^3
v	velocity, m/s
W	work, J
z	piston displacement, m

Subscripts

1	property in chamber
2	property of incoming flow value
∞	ambient conditions
A, B	chamber A and B
B	Bottom
CH	Center-Horizontal
CV	Center-Vertical
cv	control volume
D	diameter
f	friction
g	gas
I	Inner
i	node number
N	Nitrogen
O	Outer
p	piston
r	rod
s	surface
T	Top

Superscripts

'	time derivative
---	-----------------

List of Figures

2.1	The resonator	3
2.2	Sketch of the spring	4
3.1	Normal force caused by the seal.(K. Flitney and W. Brown, 2007)	9
3.2	3D-visualization of the nodes.	11
3.3	Flow chart of the program	14
4.1	Case 1 - Simulation with only metal to metal contact on the top and bottom surface of the gas spring casing.	16
4.2	Case 1 - Measured temperatures in the bottom gas spring.	16
4.3	Case 1 - Measured temperatures in the top gas spring.	17
4.4	Case 1 - Simulation with both convection and conduction on the top and bottom surface of the gas spring casing.	18
4.5	Case 1 - Simulation with adjusted friction versus measured temperatures in the top gas spring.	19
4.6	Case 1 - Simulation with adjusted friction versus measured temperatures in the bottom gas spring.	19
4.7	Case 1 - Simulated heat distribution in the gas spring after 1500s.	20
4.8	Case 1 - Simulated pressure with adjusted friction versus measured pressure in the top gas spring.	20
4.9	Case 1 - Simulated pressure with adjusted friction versus measured pressure in the bottom gas spring.	21
4.10	Case 1 - Simulation with adjusted friction run to a steady state.	21
4.11	Case 2 - Simulated temperatures with adjusted friction versus measured temperatures in the bottom spring.	22
A.1	Density as a function of temperature at constant pressure	30
C.1	Internal node	33
C.2	Node on the wall on the inside of the cylinder	34
C.3	Node on the wall on the outside of the cylinder	36
C.4	Node on the bottom/top of the cylinder	37
C.5	Node at an internal corner on the inside of the cylinder	38
C.6	Node at an internal corner on the outside of the cylinder	39
C.7	Node at an external corner on the inside of the cylinder	41
C.8	Node at an external corner on the outside of the cylinder	42

D.1	The graphical user interface.	44
-----	---------------------------------------	----

List of Tables

3.1	Frictional data for the piston seal	9
3.2	Finite difference equations	12
4.1	The input values for the different cases investigated.	15
B.1	Areas and volumes used in equation (3.28) to (3.34)	31
B.1	Areas and volumes used in equation (3.28) to (3.34)	32
E.1	Simulations performed and test results received.	45
E.1	Simulations performed and test results received.	46
E.1	Simulations performed and test results received.	47

Chapter 1

Introduction

The International Energy Agency estimates that by 2050 the geothermal electricity generation could reach 1400 TWh per year, i.e. 3.5% of the global energy production (Beerepoot, 2011, p. 19). To reach that level of production the cost of geothermal electricity has to decrease, and the development of new and more efficient drilling technology is a key parameter to reduce the cost.

“Drilling costs constitute a substantial portion of the total cost of geothermal energy. Thus, the performance of the whole geothermal industry stands to improve – and a larger portion of the geothermal resource would become economically accessible – if drilling costs could be dramatically reduced and supplemented by improved drilling methods and novel exploration techniques.”
(Beerepoot, 2011, p. 26)

Improved drilling efficiency is also one of four business critical technologies identified by Statoil to reach their growth ambitions. They have a goal to reduce the well construction time and cost with 30 and 15 per cent respectively by 2020. Considering their annual drilling costs of around 50 billion Norwegian kroner, the savings would be considerable (Statoil, 2012).

To address these challenges Resonator AS is developing a hammer drilling system suitable for oil and geothermal drilling. Their core technology consists of a linear engine that acts as a piston moving up and down between two springs inside its casing. The motion of the piston causes the casing to pound like a hammer.

The system has been tested with mechanical springs to find that the spring fails due to fatigue. As a consequence Resonator AS have chosen to use pneumatic springs. The high pressure in the pneumatic springs introduce the need for a sealing. The sealing mechanism produces friction and therefore frictional heat. It is of interest to estimate the extent of the frictional heat, as the seals that are installed can operate in a limited range of pressure and temperature.

A dynamic model has been developed to predict the behavior of the gas properties under influence of frictional heating, this has been done using control volumes techniques. Special attention has been given to the heat transfer between the gas and the parts of the gas spring. To be able to model the heat transfer in two dimensions it was necessary to derive heat transfer equations for an axis-symmetric system in cylindrical coordinates.

The model was implemented in a MATLAB-code, and a graphical user interface developed to enable use of the program by users unfamiliar with the code. Finally a comparison between test results and the simulation results was carried out to validate the model.

Chapter 2

System description

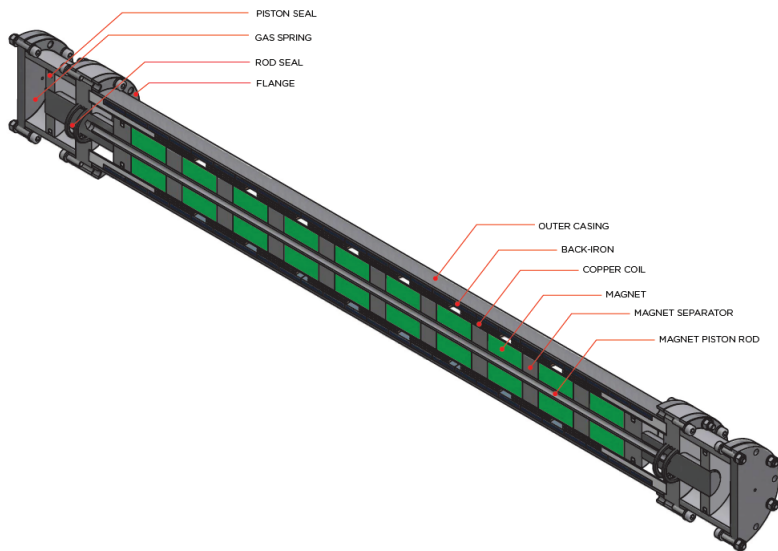


Figure 2.1: The resonator

The prototype resonator is shown in figure 2.1. In the center of the device there is a magnet piston that is driven by a magnetic field. This is created in the coil by electric currents. On each side of the linear engine there is a pneumatic spring. The motion of the casing caused by the magnet piston moving between the springs make it well suited for hammer drilling, which is the intended use of the device.

When the device is running the gas in the chambers is compressed and decompressed by the moving piston. This movement also leads to frictional heating when

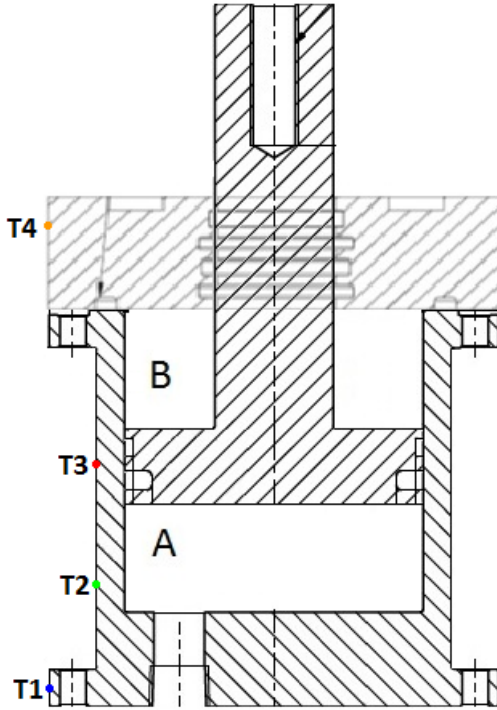


Figure 2.2: Sketch of the spring

the seal rubs against the cylinder. The seals are fit for use in temperatures between -45°C and 200°C and the seals have a lifetime of 2 million cycles (Trelleborg Sealing Solutions, 2011). The main motivation for developing this model is to predict whether the seals will fail prematurely.

The spring to be modeled is shown in figure 2.2. The bottom chamber is referred to as chamber A while the top chamber is referred to as chamber B. T1-T4 show the placement of the thermocouples used to measure the surface temperatures on the device.

It was stated in the original system description from Resonator that both chamber A and B contained pressurized gas and that a rod and a piston seal was installed to prevent pressure loss to the surroundings and between the chambers respectively. The model was developed based on that information. However, the device at Resonators work shop is running with only chamber A pressurized and no rod seal installed. To be able to compare the simulations with test results the model has been modified to reflect the actual operating conditions.

Chapter 3

Modeling

The steady state temperature will be determined by treating each of the chambers in the pneumatic spring as control volumes and solve the energy balance for the temperature. Ignoring potential and kinetic energy the following energy balance is obtained.

$$\frac{dU_{cv}}{dt} = \dot{Q}_{cv} - \dot{W}_{cv} + \Delta H \quad (3.1)$$

The density of the nitrogen in the chambers will be determined by differentiating $m = \rho V$ with respect to time and solving for $\frac{\partial \rho}{\partial t}$.

$$\frac{\partial \rho}{\partial t} = \frac{\frac{\partial m}{\partial t} - \rho \frac{\partial V}{\partial t}}{V} \quad (3.2)$$

In addition the ideal gas law will be used to obtain the pressure in the chambers.

$$p = \rho RT \quad (3.3)$$

3.1 Assumptions and simplifications

The following assumptions and simplifications have been made:

- Flat energy profile is assumed. The thermodynamical properties of the gas are considered uniform throughout the control volume.
- Isentropic flow is assumed over the seal orifice.
- The seal friction is assumed to pass as heat directly into the chamber wall and rod.
- The piston and the cylinder exchange heat by conduction through the lubrication oil.

- Since the top and bottom surface of the cylinder and the piston rod is connected to other parts it is assumed that $Q_{in} = Q_{out}$ where there is metal to metal contact in the z-direction.
- Ideal gas is assumed. Under the conditions investigated the deviations from ideal gas behavior are assumed negligible. At high pressure and low temperature there may be some deviation from this, since nitrogen is a real gas. A comparison of ideal gas versus real gas can be found in appendix A.

3.2 Volume and piston velocity

The piston oscillates with a frequency f and has a maximum amplitude B . Knowing that the displacement is described by a sine wave gives the following function for the displacement of the piston,

$$z = B \sin(\omega t) \quad (3.4)$$

where $\omega = 2\pi f$. The piston velocity is found by differentiating equation (3.4) with respect to time.

$$v = \omega B \cos(\omega t) \quad (3.5)$$

The displacement is used to express the volume of the chambers as a function of time.

$$V_A = r_p^2 \pi (L + z) \quad (3.6)$$

$$V_B = (r_r^2 - r_p^2) \pi (L - z) \quad (3.7)$$

Equations (3.8) and (3.9) are obtained by differentiating equation (3.6) and (3.7) with respect to time. It is recognized that only z is a function of time, and that its time derivative is v .

$$\frac{\partial V_A}{\partial t} = r_p^2 \pi v \quad (3.8)$$

$$\frac{\partial V_B}{\partial t} = (r_r^2 - r_p^2) \pi v \quad (3.9)$$

3.3 Leakage flow

The leakage flow is found by following the derivation done by Rogers and Mayhew (1992, p. 420-425). It is assumed that the leakage flow is isentropic, i.e. $dq = 0$, so that the energy equation becomes the following.

$$de = dh + d\left(\frac{1}{2}v^2\right) \quad (3.10)$$

Integrating equation (3.10) and using the isentropic relation $\frac{p}{\rho^\gamma} = \text{constant}$ and $dh = \frac{dp}{\rho}$ to get equation (3.11), assuming that energy is conserved.

$$\frac{1}{2}(v_2^2 - v_1^2) = \frac{\gamma}{1 - \gamma} \left(\frac{p_2}{\rho_2} - \frac{p_1}{\rho_1} \right) \quad (3.11)$$

Here the subscript 1 and 2 refer to the chamber and the opening respectively. The flow under consideration is from a large reservoir through a small opening. Hence the velocity in the reservoir is negligible compared to the velocity through the opening. Neglecting v_1 and rearranging knowing that $\frac{p}{\rho^\gamma}$ is constant and $p = \rho RT$ to get an expression for the flow velocity through the seal orifice.

$$v_2 = \left[\frac{2\gamma}{1 - \gamma} RT_1 \left(\left(\frac{p_2}{p_1} \right)^{\frac{\gamma-1}{\gamma}} - 1 \right) \right]^{\frac{1}{2}} \quad (3.12)$$

The mass flow can now be found by using that $\dot{m} = \rho v_2 A$.

$$\dot{m} = p_1 A \left[\frac{2\gamma}{1 - \gamma} \frac{1}{RT_1} \left(\left(\frac{p_2}{p_1} \right)^{\frac{\gamma+1}{\gamma}} - \left(\frac{p_2}{p_1} \right)^{\frac{2}{\gamma}} \right) \right]^{\frac{1}{2}} \quad (3.13)$$

The pressure ratio needed to achieve choked flow is found to be $\frac{p_2}{p_1} = 0.528282$ from isentropic flow tables for an ideal gas with $\gamma = 1.4$. Resonator specified a maximum pressure leakage of 1% per hour over the piston and no leakage over the rod seal. Knowing that, the maximum leakage flow is calculated using the initial conditions.

$$\dot{m}_{max} = \frac{0.01}{3600} \frac{pV}{RT} \quad (3.14)$$

3.4 Enthalpy and Internal energy

To solve the energy equation for temperature the left hand side of equation (3.1) is factorized using $U = mu$.

$$\frac{\partial U}{\partial t} = \frac{\partial}{\partial t}(mu) = \dot{m}u + mc_v \frac{\partial T}{\partial t} \quad (3.15)$$

Internal energy is generally used to determine differences, not absolute values (Rogers and Mayhew, 1992, p. 22), it is therefore of interest to get rid of u in the first term on the right hand side of equation (3.15). By recognizing that $u = u_1$ since a flat energy profile is assumed equation (3.16) is obtained.

$$\dot{m}u = (\dot{m}_2 - \dot{m}_1)u_1 \quad (3.16)$$

$$\dot{m}\Delta h = \dot{m}_2 h_2 - \dot{m}_1 h_1 \quad (3.17)$$

Equation (3.18) is obtained by subtracting equation (3.16) from the enthalpy, i.e. equation (3.17), and using the fact that $h = u + \frac{p}{\rho}$.

$$\begin{aligned} \dot{m}_2 h_2 - \dot{m}_1 h_1 - (\dot{m}_2 - \dot{m}_1)u_1 = \\ \dot{m}_2(h_2 - h_1) - \frac{p}{\rho}(\dot{m}_2 - \dot{m}_1) \end{aligned} \quad (3.18)$$

By recognizing that $\dot{m}_1 = 0$ and that $\dot{m}\Delta h = c_p \Delta T$ equation (3.19) is obtained.

$$\dot{m}\Delta h - \dot{m}u = \dot{m}c_p(T_2 - T_1) - \frac{p}{\rho}\dot{m} \quad (3.19)$$

3.5 Friction

The friction contributes to the heating of the system and it is necessary to estimate the extent of this heat. As can be seen in figure 3.1 the O-ring is inserted in to the groove with an initial compression causing an initial normal force $N = p_0 A$.

The compression of the O-ring in the x-direction by the pressure makes it expand in the normal direction, hence increasing the normal force. The normal force exerted by the seal on the wall is a linear function of the pressure given by equation (3.20).

$$N = A(p_0 + p) \quad (3.20)$$

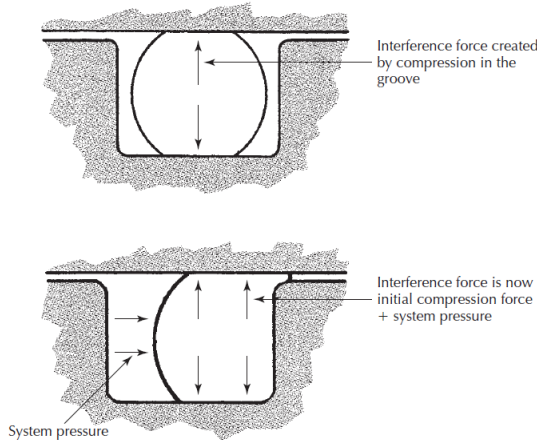


Figure 3.1: Normal force caused by the seal.(K. Flitney and W. Brown, 2007)

Table 3.1: Frictional data for the piston seal

Pressure	Friction force	Friction coefficient	Normal force
30	110	0.145	728
150	190	0.126	1526
330	260	0.097	2723

The friction force can be found by using equation (3.21). However, the friction coefficient changes with pressure since the seal material will be deformed and the surface characteristics altered with changing normal force. The velocity also affects the friction coefficient as the thickness of the lubrication film varies with speed. When the lubrication film is thicker than the roughness of the seal surface the friction is reduced since the contact area between the surfaces is reduced. (K. Flitney and W. Brown, 2007, p. 294-296).

$$F_f = \mu_k N \tag{3.21}$$

Table 3.1 is provided by the seal manufacturer, Trelleborg Sealing Solutions. The data shows how the friction between the piston seal and the cylinder wall changes with pressure at a velocity of 10m/s, provided there is an oil film present. It is likely that the equations derived from the given data will produce a friction force greater than the real friction since 10m/s is the maximum piston velocity. However, applying a higher friction force will produce a conservative answer, which is to be preferred compared to an underestimated erroneous answer.

The normal force is expected to be a linear function of the pressure, and so is the friction coefficient since the values are given for a constant velocity. It is also expected that the friction force is a linear function of the normal force times the

friction coefficient.

Averaging the gradients between the data points gives the following equations for the normal force, friction coefficient and friction force respectively. *Be aware that the equations are only valid if the pressures are given in bar.*

$$N = 528.5 + 6.65p \quad (3.22)$$

$$\mu_k = 0.1498 - 0.00016p \quad (3.23)$$

$$F_f = 8.7 + 0.95\mu_k N \quad (3.24)$$

The rate of frictional heat generation is a product of force times relative velocity between the moving parts as identified by equation (3.25) below.

$$\dot{Q}_f = F_f v \quad (3.25)$$

There is no available data for the rod seal, therefore a ratio between seal areas is used to estimate the heat generated by friction between the rod and the seal.

3.6 Heat Transfer

The heat transfer between the gas and the cylinder/piston happens through convection. To determine the heat transfer it is necessary to know the surface temperatures on the device. Text books like Heat Transfer by Holman (2002, p. 86-87 and 94) and Fundamentals of Heat and Mass Transfer by P. Incopera et al. (2007, p. 306) gives the finite difference equations for simple geometries with uniform grids. However, for the geometry dealt with in this problem where a radial system with a non-uniform grid in the r-direction was considered it was necessary to derive the equations.

Figure 3.2 illustrates the geometry of the nodes. The left hand side shows a 3D representation of a node while the right hand side shows the different kind of nodes present in the system. By removing colored blocks on the left hand side so that they match the colors on the right hand side of the figure, one can get an understanding of how the different nodes look like in 3D.

To derive the equations the geometry was discretized and the heat balance method described by P. Incopera et al. (2007, p. 215-217) was applied about a control volume surrounding each node. Equation (3.26) shows the energy balance used to derive the equations.

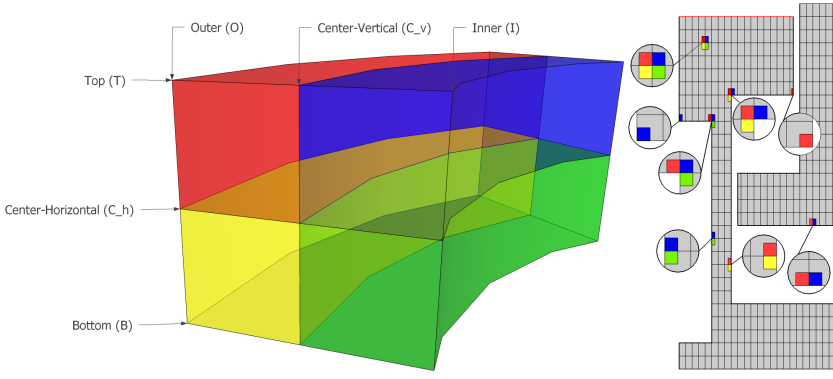


Figure 3.2: 3D-visualization of the nodes.

$$\dot{E}_{st} = \dot{E}_{in} + \dot{E}_g \quad (3.26)$$

In the above equation \dot{E}_{st} represents the rate of energy stored within the control volume, \dot{E}_{in} represents the rate of heat that enters the control volume either as conduction or as convection while \dot{E}_g represents the rate of energy generated at the surface by the friction. The conduction is given by Fourier's law while the convection is given by Newton's law of cooling. This was inserted in to equation 3.26 to give the following equation for the rate of heat transfer in two dimensions.

$$\rho cV \frac{dT}{dt} = kA \frac{dT}{dz} + kA \frac{dT}{dr} + hA\Delta T + \dot{Q}_f \quad (3.27)$$

The full derivation is shown in appendix C and all the equations for the different nodes can be found in table 3.2. The areas used in the equations can be found in appendix B.




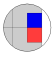



When all the surface temperatures are known the total rate of heat transfer between the gas and the spring can be found by summing the rate of heat transfer from each of the node surfaces in contact with the gas.

$$\dot{Q} = h \sum A_i (T_i - T_g) \quad (3.35)$$

3.7 Energy equation

Equation (3.1) is solved for $\frac{\partial T_g}{\partial t}$ and equation (3.19) is inserted to obtain the differential equations for the gas temperature in chamber A and B respectively, knowing that $\dot{W} = p \frac{\partial V}{\partial t}$ and $c_v = c_p - R$.

Table 3.2: Finite difference equations

Configuration	Finite difference equation
	$\frac{dT}{dt} = \frac{\alpha}{V} \left[A_O \frac{T_{i+1,j} - T_{i,j}}{r_{i+1} - r_i} + A_I \frac{T_{i-1,j} - T_{i,j}}{r_i - r_{i-1}} + A_T \frac{T_{i,j+1} - T_{i,j}}{\Delta z} + A_B \frac{T_{i,j-1} - T_{i,j}}{\Delta z} \right] \quad (3.28)$
	$\frac{dT}{dt} = \frac{\alpha}{V} \left[A_O \frac{T_{i+1,j} - T_{i,j}}{r_{i+1} - r_i} + A_T \left(\frac{T_{i,j+1} - T_{i,j}}{\Delta z} + \frac{T_{i,j-1} - T_{i,j}}{\Delta z} \right) + \frac{h_{ACV}}{\rho cV} (T_\infty - T_{i,j}) + \frac{\dot{Q}_f}{2\pi \rho cV} \right] \quad (3.29)$
	$\frac{dT}{dt} = \frac{\alpha}{V} \left[A_I \frac{T_{i-1,j} - T_{i,j}}{r_i - r_{i-1}} + A_T \left(\frac{T_{i,j+1} - T_{i,j}}{\Delta z} + \frac{T_{i,j-1} - T_{i,j}}{\Delta z} \right) + \frac{h_{ACV}}{\rho cV} (T_\infty - T_{i,j}) + \frac{\dot{Q}_f}{2\pi \rho cV} \right] \quad (3.30)$
	$\frac{dT}{dt} = \frac{\alpha}{V} \left[A_O \frac{T_{i+1,j} - T_{i,j}}{r_{i+1} - r_i} + A_I \frac{T_{i-1,j} - T_{i,j}}{r_i - r_{i-1}} + A_T \frac{T_{i,j+1} - T_{i,j}}{\Delta z} + \frac{h_{ACH}}{\rho cV} (T_\infty - T_{i,j}) \right] \quad (3.31)$
	$\frac{dT}{dt} = \frac{\alpha}{V} \left[A_O \frac{T_{i+1,j} - T_{i,j}}{r_{i+1} - r_i} + A_I \frac{T_{i-1,j} - T_{i,j}}{r_i - r_{i-1}} + A_T \frac{T_{i,j+1} - T_{i,j}}{\Delta z} + A_B \frac{T_{i,j-1} - T_{i,j}}{\Delta z} \right] + \frac{h(T_\infty - T_{i,j})}{\rho cV} (A_{CV} + A_{CH}) \quad (3.32)$
	$\frac{dT}{dt} = \frac{\alpha}{V} \left[A_O \frac{T_{i+1,j} - T_{i,j}}{r_{i+1} - r_i} + A_T \frac{T_{i,j+1} - T_{i,j}}{\Delta z} \right] + \frac{h(T_\infty - T_{i,j})}{\rho cV} (A_{CV} + A_{CH}) \quad (3.33)$
	$\frac{dT}{dt} = \frac{\alpha}{V} \left[A_I \frac{T_{i-1,j} - T_{i,j}}{r_i - r_{i-1}} + A_T \frac{T_{i,j+1} - T_{i,j}}{\Delta z} \right] + \frac{h(T_\infty - T_{i,j})}{\rho cV} (A_{CV} + A_{CH}) \quad (3.34)$

$$\frac{\partial T_{gA}}{\partial t} = \frac{\dot{Q}_A - p \frac{\partial V_A}{\partial t} + \dot{m} c_p (T_{gB} - T_{gA}) - \frac{p_A}{\rho_A} \dot{m}_A}{m_A (c_p - R)} \quad (3.36)$$

$$\frac{\partial T_{gB}}{\partial t} = \frac{\dot{Q}_B - p_b \frac{\partial V_B}{\partial t} + \dot{m} c_p (T_{gA} - T_{gB}) - \frac{p_B}{\rho_B} \dot{m}_B}{m_B (c_p - R)} \quad (3.37)$$

In practice chamber B is unpressurized and there is no rod seal. To adapt the model to this configuration the pressure and temperature in chamber B was set to ambient conditions. In addition the leakage flow in equation 3.36 was set to $\dot{m} = 0$ leading to the following equations for the density and temperature in chamber A.

$$\frac{\partial \rho}{\partial t} = \frac{-\rho \frac{\partial V}{\partial t}}{V} \quad (3.38)$$

$$\frac{\partial T_{gA}}{\partial t} = \frac{\dot{Q}_A - p \frac{\partial V_A}{\partial t}}{m_A (c_p - R)} \quad (3.39)$$

The differential equations are solved using a numerical integrator, in this case the Runge-Kutta solver used in MATLAB's ode45. The flow chart in figure 3.3 shows the algorithm used to solve the equations, and a description of the program can be found in appendix D.

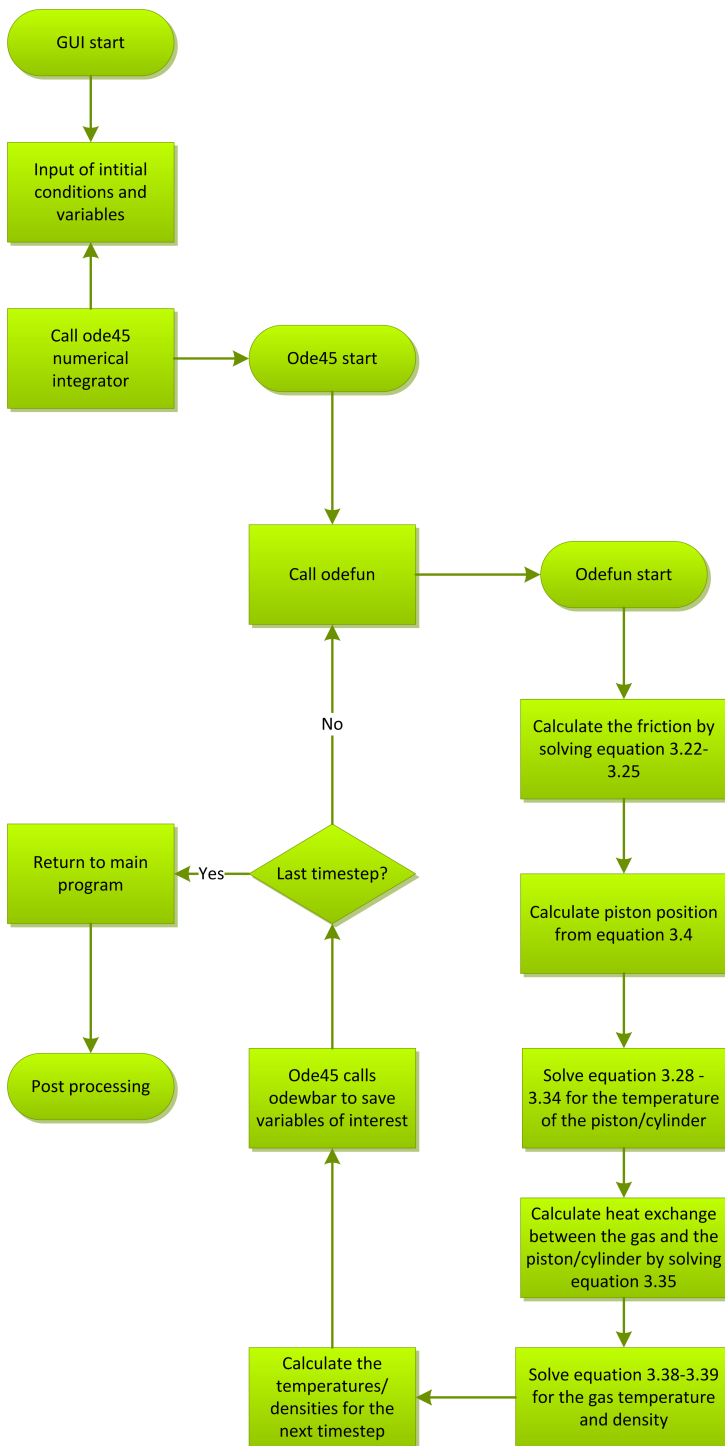


Figure 3.3: Flow chart of the program

Chapter 4

Results and discussion

Two cases have been investigated to verify that the model produces results consistent with reality. The first case is used to tune the friction levels so that the simulation results reflect the test results. The second case is used to determine if the tuned friction will describe the physics correctly for a different set of input values. A table summarizing the simulations can be found in appendix E.

Table 4.1: The input values for the different cases investigated.

	Amplitude [mm]	Initial Pressure [bar]	Frequency [Hz]
Case 1	2	30	75
Case 2	3.5	51	94

4.1 Case 1

Figure 4.1 shows the simulated temperatures for case 1 with the input values from table 4.1.

In the simulation T3 increase rapidly. This is a reasonable result since the temperature is measured by the thermocouple closest to the center position of the piston. The piston oscillates about the center position where it has its maximum velocity. Therefore the frictional heat input will be at its maximum at the center position. The thermocouple placed further away from the center, T2, also show an increase but a lot less than T3, while the thermocouples placed at the flange and bottom show almost no increase.

Figures 4.2 and 4.3 shows the measured surface temperatures on the bottom and top gas spring respectively.

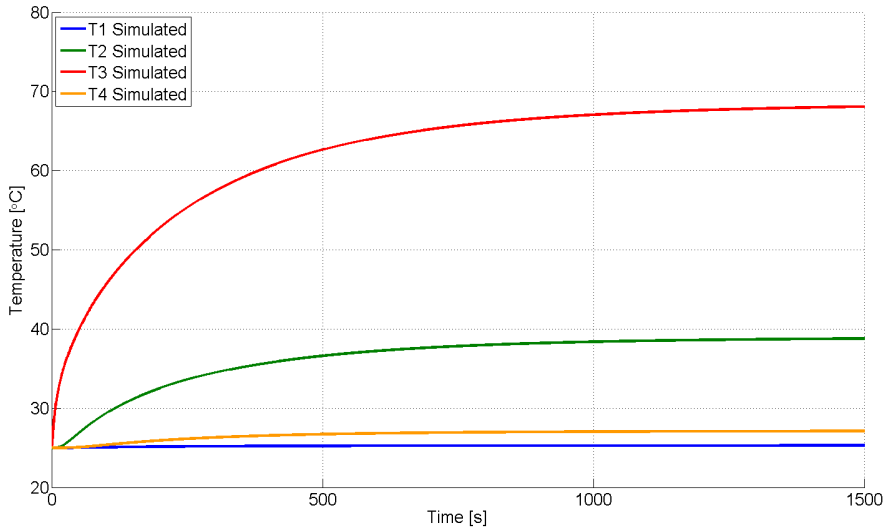


Figure 4.1: Case 1 - Simulation with only metal to metal contact on the top and bottom surface of the gas spring casing.

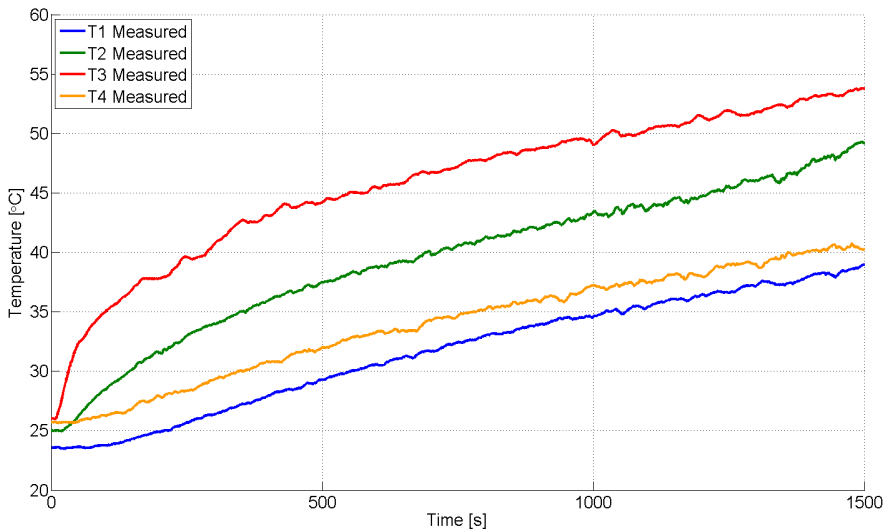


Figure 4.2: Case 1 - Measured temperatures in the bottom gas spring.

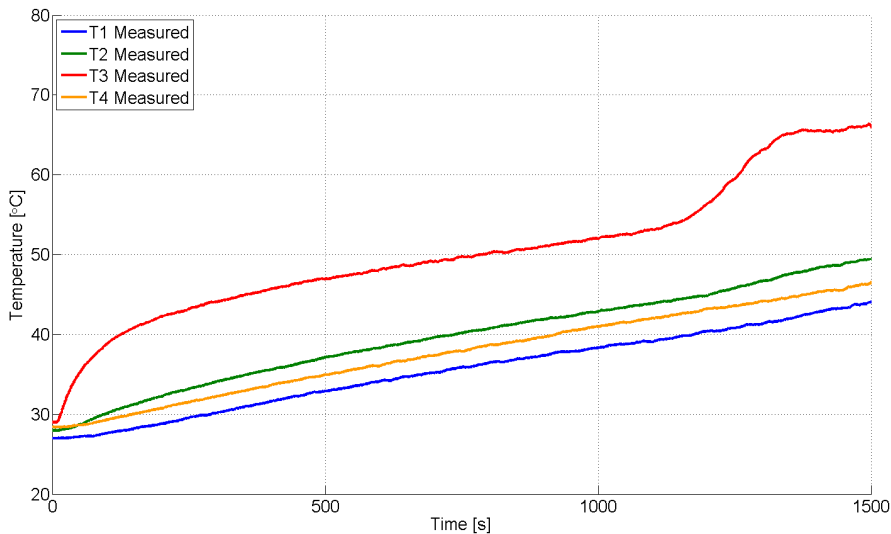


Figure 4.3: Case 1 - Measured temperatures in the top gas spring.

In the test results it can be observed that T2 and T3 increase at the beginning, with a lower gradient, but similar to the simulation. One can also observe that after the initial temperature jump the temperatures increase almost linearly with time. This is different from the simulation and may be explained by an assumption made when developing the model. For simplicity the top and bottom surface of the gas spring was modeled as if there was full metal to metal contact between the spring and the connected parts. This most likely lead to a greater amount of heat leaving the spring in the simulation than in reality. Therefore changes were made to implement both conduction and convection at those surfaces.

Figure 4.4 shows the simulation results after the change of the model. The temperatures now show a behavior similar to the test results. However, the simulation shows a higher temperature increase than the test. It was therefore necessary to adjust the friction levels to achieve better accordance with the test results.

Trelleborg Sealing Solution was contacted and new frictional data was provided. This data describe the regular GlydRing which have a greater area than the GlydRing Hz used in the spring. This leads to a lower friction for the GlydRing Hz in accordance with equations (3.20) and (3.21). The procedure used in section 3.5 was repeated, and the result multiplied with a ratio of areas to obtain equation (4.1).

$$N = 528 \frac{A_{act}}{A} + A_{act} p \quad (4.1)$$

This was implemented in the model and A_{act} adjusted to obtain the temperatures shown in figures 4.5 and 4.6. It can be observed that the simulation gives a fairly

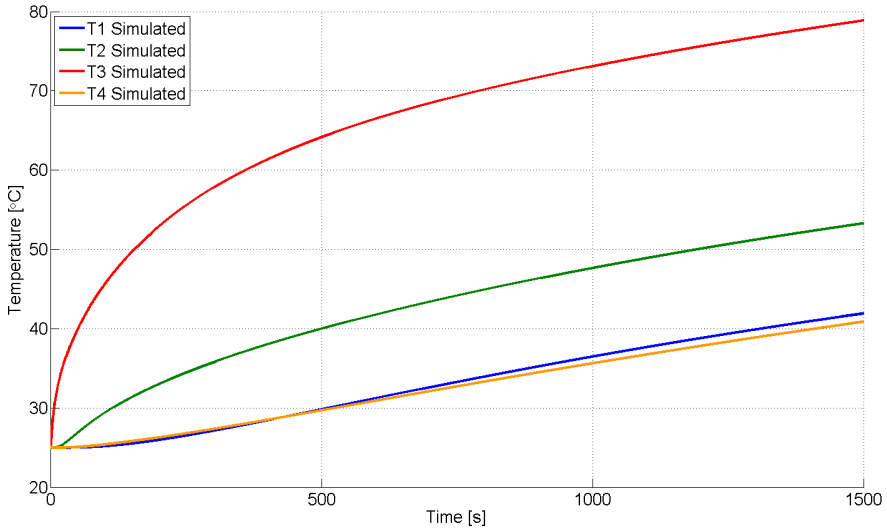


Figure 4.4: Case 1 - Simulation with both convection and conduction on the top and bottom surface of the gas spring casing.

accurate estimate of T1, T2 and T4 while T3 is about $15 - 20^{\circ}\text{C}$ higher. By looking at figure 4.7 one can see that there's a relatively large temperature gradient in the z-direction. The node that is 1.2 cm away from the center node is approximately 11°C colder than T3. This might explain the difference between the simulation and the measurements, since it is challenging to place the thermocouple with millimeter precision and the piston might be a bit off center.

Figures 4.8 and 4.9 show the simulated pressure versus the measured pressure in the top and bottom spring respectively. Both the measured pressures have a higher increase than the simulated pressure. This might indicate that the gas gets a higher heat input in reality than what is the case in the simulation. It has been assumed that the cylinder exchanges heat with the piston through the lubrication oil and that the gas in chamber B is at ambient conditions. These assumptions might differ from reality and should be investigated by measuring the surface temperatures on the inside of the gas spring.

Figure 4.10 shows that T3 and T2 reach a steady temperature below 90°C and 70°C respectively, while T1 and T4 reach as steady temperature below 60°C . All of these temperatures are below the maximum operating temperature of the seal, indicating that the seal would not fail under these operating conditions. It was not possible to provide a steady state comparison through lack of experimental test data.

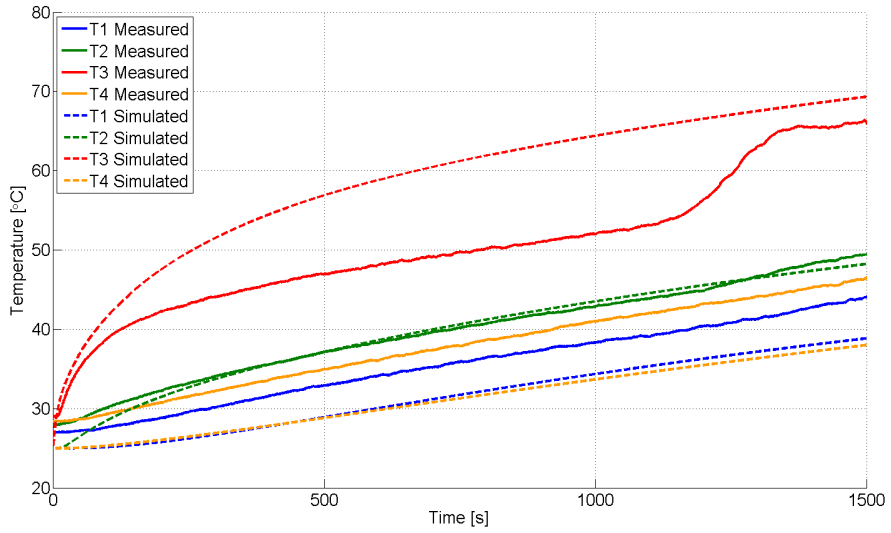


Figure 4.5: Case 1 - Simulation with adjusted friction versus measured temperatures in the top gas spring.

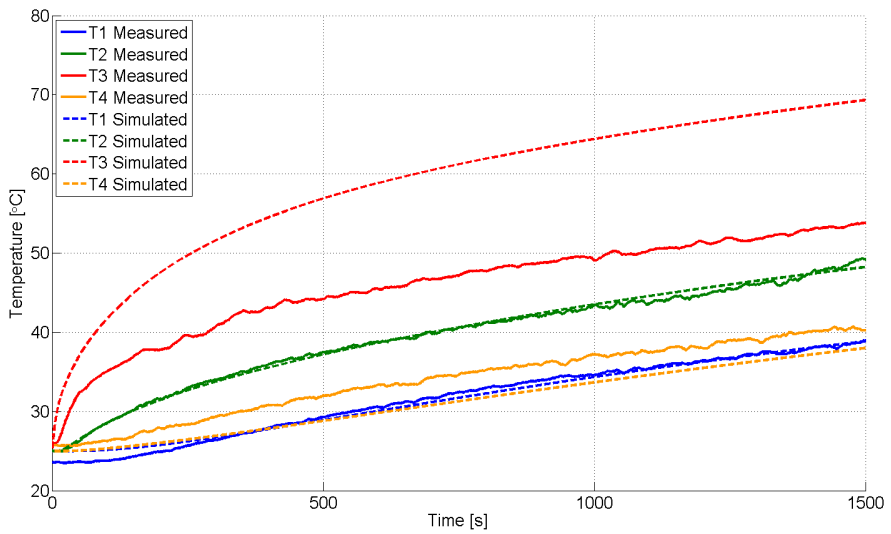


Figure 4.6: Case 1 - Simulation with adjusted friction versus measured temperatures in the bottom gas spring.

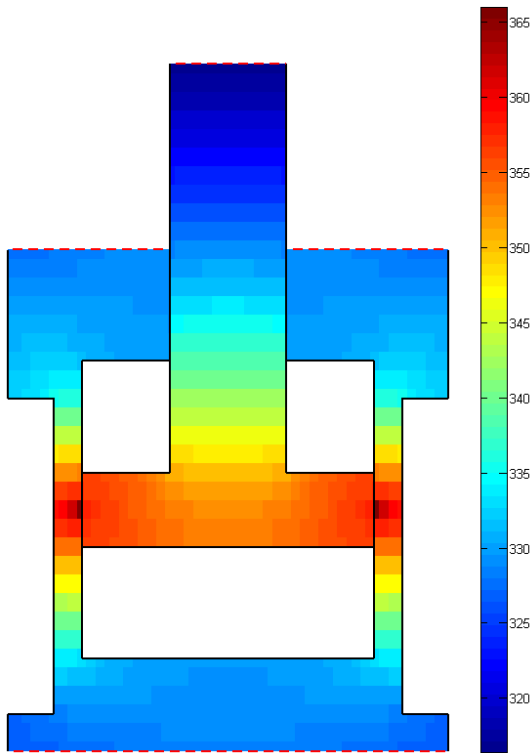


Figure 4.7: Case 1 - Simulated heat distribution in the gas spring after 1500s.

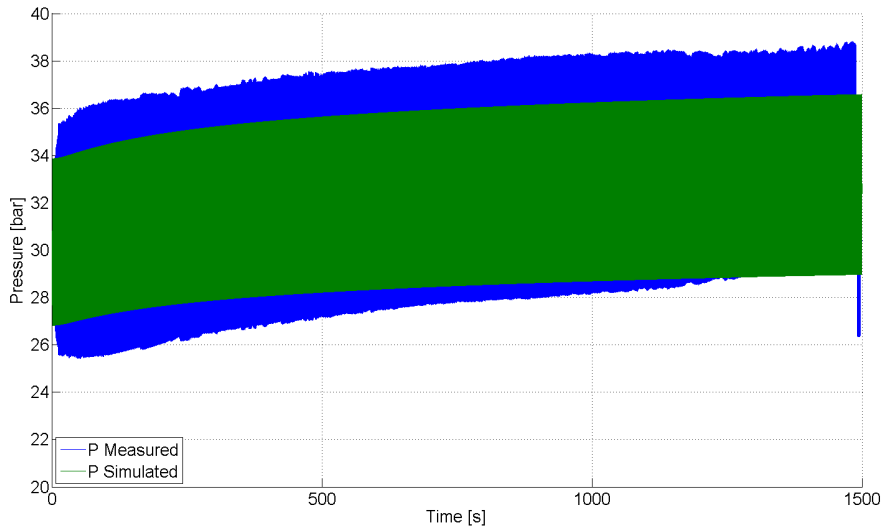


Figure 4.8: Case 1 - Simulated pressure with adjusted friction versus measured pressure in the top gas spring.

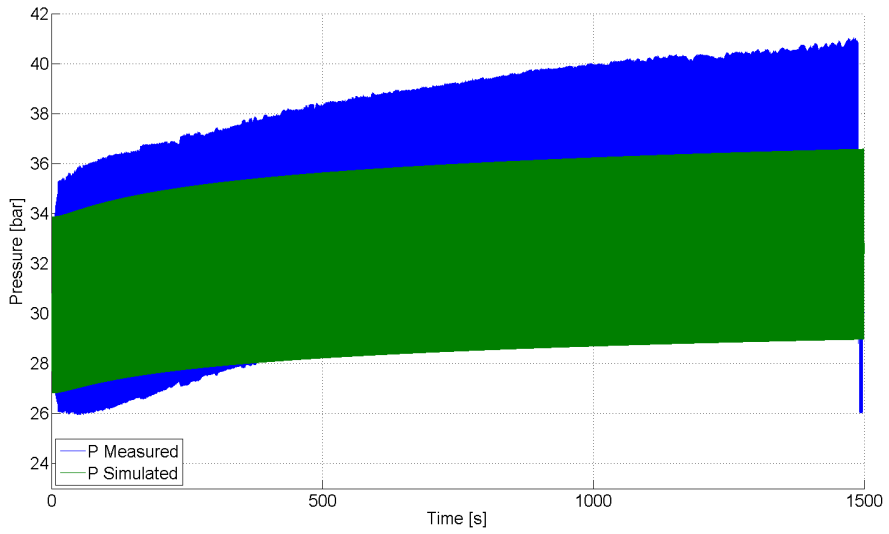


Figure 4.9: Case 1 - Simulated pressure with adjusted friction versus measured pressure in the bottom gas spring.

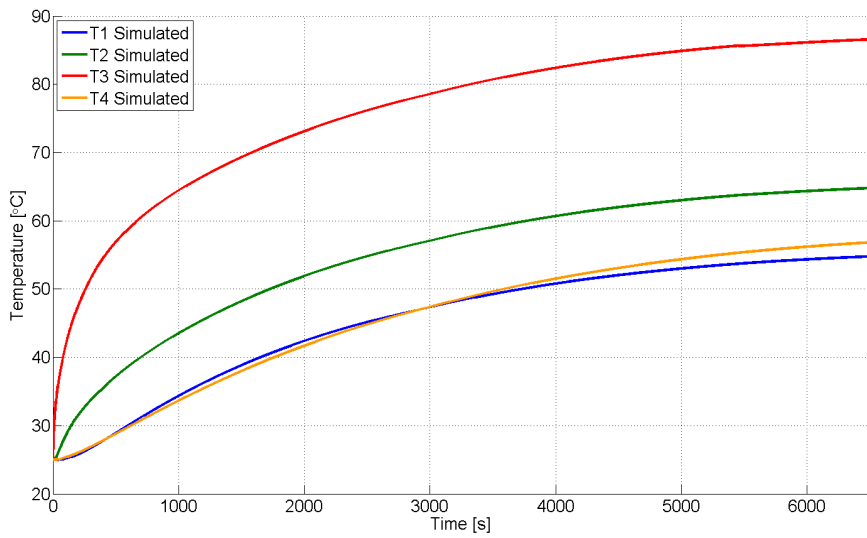


Figure 4.10: Case 1 - Simulation with adjusted friction run to a steady state.

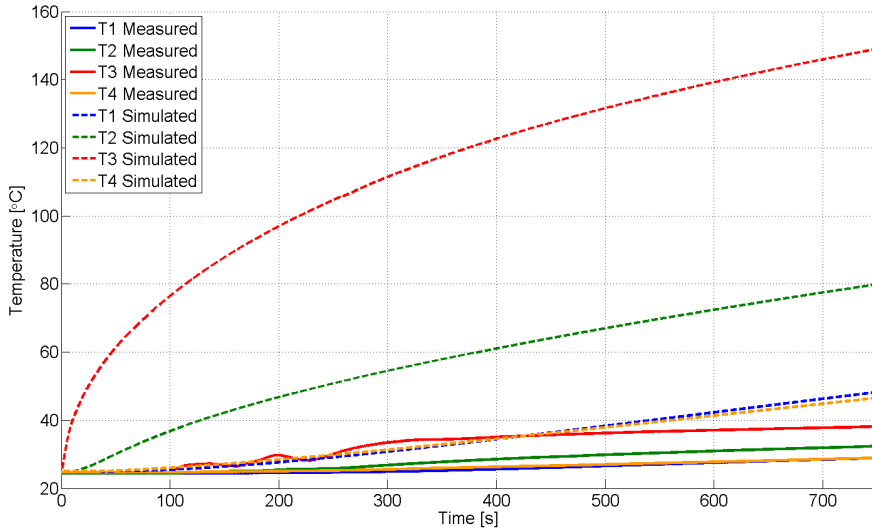


Figure 4.11: Case 2 - Simulated temperatures with adjusted friction versus measured temperatures in the bottom spring.

4.2 Case 2

Figure 4.11 shows the simulated temperatures versus the measured temperatures for case 2. It can be observed that the simulated temperatures does not match the measured temperatures when the initial conditions are changed. This suggests that the adjusted friction is not suited to describe the friction for other input values than the ones used in case 1.

4.3 Final discussion

The results of case 1 shows that the simulated temperatures have rate of change that corresponds well to the test results, suggesting that the thermal inertia of the model is approximately correct.

As mentioned in section 3.5 the friction coefficient varies with speed since the lubrication film thickness is dependent of velocity. The results of case 2 indicates that the friction coefficient used in the simulation does not reflect this velocity dependence sufficiently. The data received from the seal manufacturer is insufficient to determine the relation between the friction coefficient and the velocity. Before the model is used to draw any conclusions regarding seal performance, the velocity dependence should be investigated and implemented in model to improve its accuracy.

Chapter 5

Conclusion

The dynamic model developed in this thesis has been used to simulate the effects of friction on the gas properties and the temperature distribution in the gas spring parts. By comparing the model with test results for two sets of input values the following conclusions can be made:

- The simulations showed that the model reflects the thermal inertia of the system appropriately if friction levels are adjusted to reflect experimental data.
- The friction model used does not reflect the velocity dependence of the friction coefficient satisfactorily.

Chapter 6

Further Work

To improve the accuracy of the model the following steps should be considered:

- An improved frictional model should be implemented in the model as the present model does not reflect the velocity dependence of the friction coefficient satisfactorily. This can be done by testing the seal for a range of different pressures and velocities to determine the friction coefficient as a function of both those variables.
- Further comparison with test results should be done until the model is validated for more than one set of input values.
- A review of experimental data should be completed by Resonator AS and improvements in sampling and range of available data would help the validation process greatly.

Bibliography

- Milou Beerepoot. Technology roadmap: Geothermal heat and power. Technical report, International Energy Agency (IEA), 2011.
- Jack Phillip Holman. *Heat Transfer*. McGraw-Hill, 9th edition, 2002.
- Robert K. Flitney and Melvin W. Brown. *Seals and sealing handbook*. Elsevier/Butterworth-Heinemann, 5th edition, 2007.
- Benjamin Gayle Kyle. *Chemical and process thermodynamics*. Prentice Hall, 2nd edition, 1992.
- Frank P. Incopera, David P. DeWitt, Theodore L. Bergman, and Adrienne S. Lavine. *Fundamentals of Heat and Mass Transfer*. John Wiley & sons, 6th edition, 2007.
- Gordon Rogers and Yon Mayhew. *Engineering thermodynamics - Work and heat transfer*. Longman Scientific & Technical, 4th edition, 1992.
- Statoil. Putting technology to work - corporate technology strategy, 2012.
URL <http://www.statoil.com/no/NewsAndMedia/News/2011/Downloads/CTS-Communicationpackage-external.ppt>.
- TrelleborgSealingSolutions. *Hydraulic seals - linear*. URL http://www.tss.trelleborg.com/remotemedia/media/globalformastercontent/downloadsautomaticlycreatedbyscript/catalogs/piston_gb_en.pdf.

Appendix A

Ideal versus real gas

The last assumption in section 3.1 can be justified by comparing the ideal gas law with an equation of state based on empirical relations such as the Peng-Robinson equation of state. Kyle (1992) gives the Peng-Robinson equation of state in polynomial form.

$$Z^3 + (B - 1)Z^2 + (A - 3B^2 - 2B)Z + (B^3 + B^2 - AB) = 0 \quad (\text{A.1})$$

Where

$$Z = \frac{P}{\rho RT} \quad (\text{A.2})$$

$$A = 0.045724 \frac{P_r}{T_r^2} \left[1 + \kappa(1 - T_r^{1/2}) \right]^2 \quad (\text{A.3})$$

$$B = 0.07780 \frac{P_r}{T_r} \quad (\text{A.4})$$

$$\kappa = 0.37464 + 1.5422\omega - 0.26992\omega^2 \quad (\text{A.5})$$

In the above equations ω is the acentric factor, $P_r = \frac{P}{P_c}$ and $T_r = \frac{T}{T_c}$ is the reduced pressure and temperature while P_c and T_c is the critical pressure and temperature respectively. Figure A.1 shows a comparison of the ideal gas law and the Peng-Robinson equation. The pressures simulated are in the range 20-100 bar, where the deviations from the ideal gas law are considered negligible.

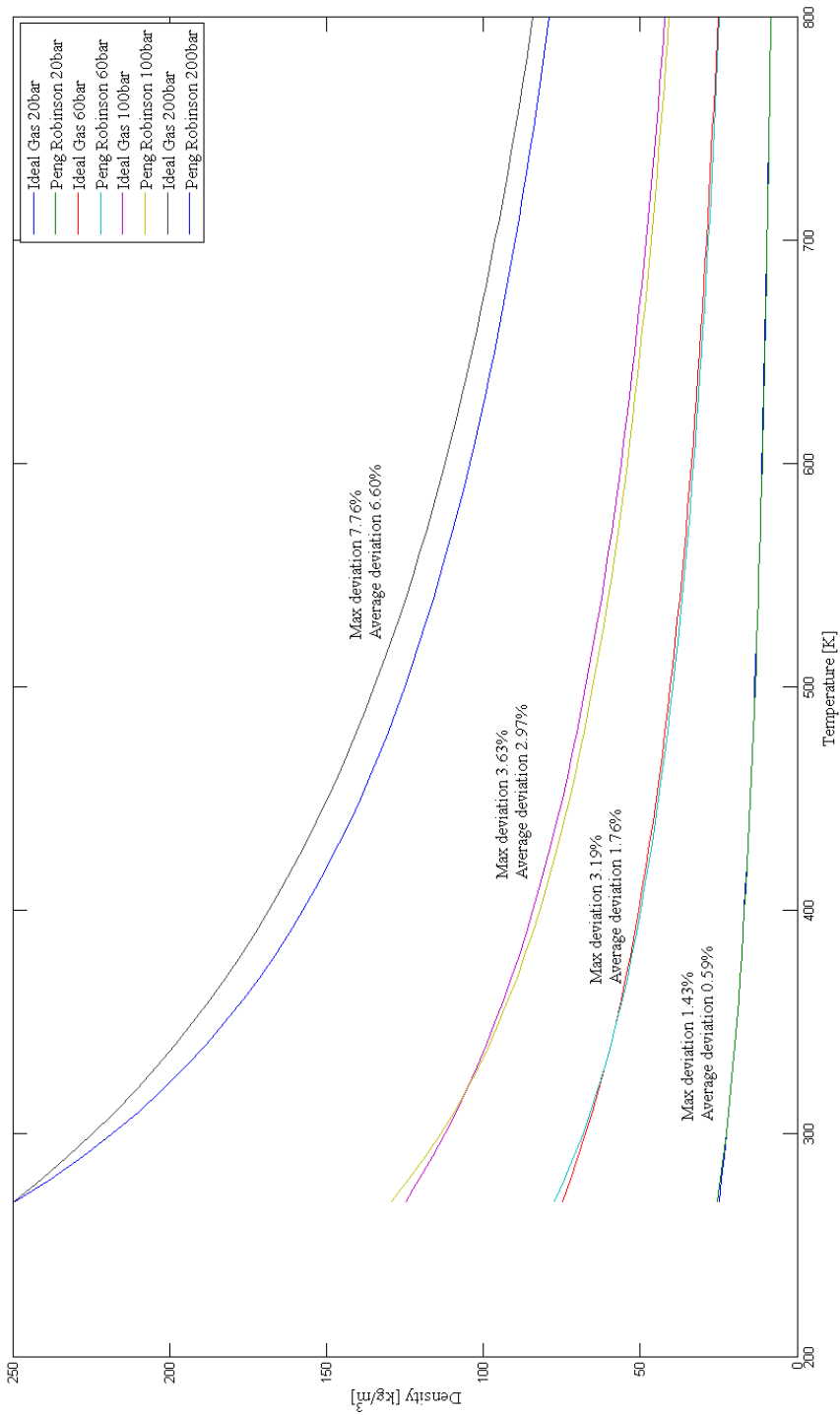


Figure A.1: Density as a function of temperature at constant pressure

Appendix B

Areas

The areas used in (3.28) to (3.34) is shown in table B.1.

Table B.1: Areas and volumes used in equation (3.28) to (3.34)


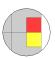

Eq. #	$\frac{Area/volume}{2\pi}$	Configuration
(3.28)	$A_O = \frac{\Delta z}{2}(r_{i+1} + r_i)$ $A_I = \frac{\Delta z}{2}(r_i + r_{i-1})$ $A_T = A_B = \frac{1}{8} [(r_{i+1} + r_i)^2 - (r_i + r_{i-1})^2]$ $V = A_T \Delta z$	
(3.29)	$A_O = \frac{\Delta z}{2}(r_{i+1} + r_i)$ $A_{CV} = r_i \Delta z$ $A_T = A_B = \frac{1}{8} [(r_{i+1} + r_i)^2 - 4r_i^2]$ $V = A_T \Delta z$	
(3.30)	$A_I = \frac{\Delta z}{2}(r_i + r_{i-1})$ $A_{CV} = r_i \Delta z$ $A_T = A_B = \frac{1}{8} [4r_i^2 - (r_i + r_{i-1})^2]$ $V = A_T \Delta z$	

Table B.1: Areas and volumes used in equation (3.28) to (3.34)

Eq. #	$\frac{Area/volume}{2\pi}$	Configuration
(3.31)	$A_O = \frac{\Delta z}{4} (r_{i+1} + r_i)$ $A_I = \frac{\Delta z}{4} (r_i + r_{i-1})$ $A_T = A_{CH} = \frac{1}{8} [(r_{i+1} + r_i)^2 - (r_i + r_{i-1})^2]$ $V = A_T \frac{\Delta z}{2}$	
(3.32)	$A_O = \frac{\Delta z}{2} (r_{i+1} + r_i)$ $A_I = \frac{\Delta z}{4} (r_i + r_{i-1})$ $A_T = \frac{1}{8} [(r_{i+1} + r_i)^2 - (r_i + r_{i-1})^2]$ $A_B = \frac{1}{8} [(r_{i+1} + r_i)^2 - 4r_i^2]$ $A_{CH} = \frac{1}{8} [4r_i^2 - (r_i + r_{i-1})^2]$ $A_{CV} = \frac{r_i \Delta z}{2}$ $V = \frac{\Delta z}{2} (A_T + A_B)$	
(3.32)	$A_O = \frac{\Delta z}{4} (r_{i+1} + r_i)$ $A_I = \frac{\Delta z}{2} (r_i + r_{i-1})$ $A_T = \frac{1}{8} [(r_{i+1} + r_i)^2 - (r_i + r_{i-1})^2]$ $A_B = \frac{1}{8} [4r_i^2 - (r_i + r_{i-1})^2]$ $A_{CH} = \frac{1}{8} [(r_{i+1} + r_i)^2 - 4r_i^2]$ $A_{CV} = \frac{r_i \Delta z}{2}$ $V = \frac{\Delta z}{2} (A_T + A_B)$	
(3.33)	$A_O = \frac{\Delta z}{4} (r_{i+1} + r_i)$ $A_{CV} = \frac{r_i \Delta z}{2}$ $A_T = A_{CH} = \frac{1}{8} [(r_{i+1} + r_i)^2 - 4r_i^2]$ $V = A_T \frac{\Delta z}{2}$	
(3.34)	$A_I = \frac{\Delta z}{4} (r_i + r_{i-1})$ $A_{CV} = \frac{r_i \Delta z}{2}$ $A_T = A_{CH} = \frac{1}{8} [4r_i^2 - (r_i + r_{i-1})^2]$ $V = A_T \frac{\Delta z}{2}$	

Appendix C

Derivation of heat equations

C.1 Equation for internal node

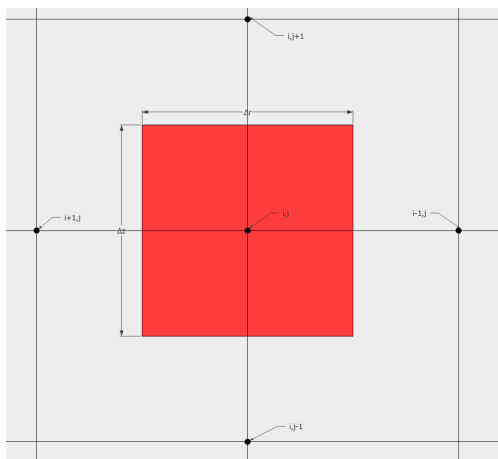


Figure C.1: Internal node

Start the derivation with the following heat balance.

$$\rho c V \frac{dT}{dt} = k A_O \left. \frac{dT}{dr} \right|_{i+1} + k A_I \left. \frac{dT}{dr} \right|_{i-1} + k A_T \left. \frac{dT}{dz} \right|_{j+1} + k A_T \left. \frac{dT}{dz} \right|_{j-1} \quad (\text{C.1})$$

Integrating to find the volume and areas. The problem is axis-symmetric so all terms are divide by 2π .

$$V = \int_{z_i - \frac{\Delta z}{2}}^{z_i + \frac{\Delta z}{2}} \int_{\frac{r_i - r_{i-1}}{2}}^{\frac{r_{i+1} + r_i}{2}} r dr dz = \frac{\Delta z}{8} ((r_{i+1} + r_i)^2 - (r_i + r_{i-1})^2) \quad (\text{C.2})$$

$$A_O = \int_{z_i - \frac{\Delta z}{2}}^{z_i + \frac{\Delta z}{2}} \left(\frac{r_{i+1} + r_i}{2} \right) dz = \frac{\Delta z}{2} (r_{i+1} + r_i) \quad (\text{C.3})$$

$$A_I = \int_{z_i - \frac{\Delta z}{2}}^{z_i + \frac{\Delta z}{2}} \frac{r_i + r_{i-1}}{2} dz = \frac{\Delta z}{2} (r_i + r_{i-1}) \quad (\text{C.4})$$

$$A_T = A_B = \int_{\frac{r_i - r_{i-1}}{2}}^{\frac{r_{i+1} + r_i}{2}} r dr = \frac{((r_{i+1} + r_i)^2 - (r_i + r_{i-1})^2)}{8} \quad (\text{C.5})$$

Solve for $\frac{dT}{dt}$, and replace the spatial derivatives with forward and backward differences.

$$\begin{aligned} \frac{dT}{dt} = \frac{\alpha}{V} \left[A_O \frac{T_{i+1,j} - T_{i,j}}{r_{i+1} - r_i} + A_I \frac{T_{i-1,j} - T_{i,j}}{r_i - r_{i-1}} \right. \\ \left. + A_T \frac{T_{i,j+1} - T_{i,j}}{\Delta z} + A_B \frac{T_{i,j-1} - T_{i,j}}{\Delta z} \right] \quad (\text{C.6}) \end{aligned}$$

C.2 Equation for node on the wall on the inside of the cylinder

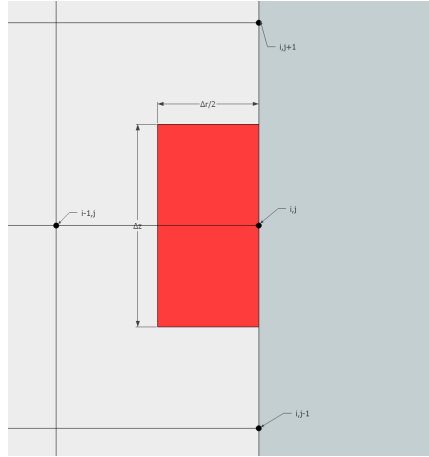


Figure C.2: Node on the wall on the inside of the cylinder

Start the derivation with the following heat balance.

$$\begin{aligned} \rho c V \frac{dT}{dt} = k A_O \frac{dT}{dr} \Big|_{i+1} + k A_T \frac{dT}{dz} \Big|_{j+1} + k A_B \frac{dT}{dz} \Big|_{j-1} \\ + h A_{CV} \Delta T + \frac{Q_{fric}}{2\pi} \quad (\text{C.7}) \end{aligned}$$

Where $Q_{fric} = 0$ if there is no friction. Integrating to find the volume and areas. The problem is axis-symmetric so all terms are divide by 2π .

$$V = \int_{z_i - \frac{\Delta z}{2}}^{z_i + \frac{\Delta z}{2}} \int_{r_i}^{\frac{r_{i+1} + r_i}{2}} r dr dz = \frac{\Delta z \left((r_{i+1} + r_i)^2 - 4r_i^2 \right)}{8} \quad (C.8)$$

$$A_O = \int_{z_i - \frac{\Delta z}{2}}^{z_i + \frac{\Delta z}{2}} \left(\frac{r_{i+1} + r_i}{2} \right) dz = \frac{\Delta z (r_{i+1} + r_i)}{2} \quad (C.9)$$

$$A_T = A_B = \int_{r_i}^{\frac{r_{i+1} + r_i}{2}} r dr = \frac{\left((r_{i+1} + r_i)^2 - 4r_i^2 \right)}{8} \quad (C.10)$$

$$A_{CV} = r_i \int_{z_i - \frac{\Delta z}{2}}^{z_i + \frac{\Delta z}{2}} dz = r_i \Delta z \quad (C.11)$$

Solving for $\frac{dT}{dt}$ and replace the derivatives with forward and backward differences.

$$\begin{aligned} \frac{dT}{dt} = \frac{\alpha}{V} & \left[A_O \frac{T_{i+1,j} - T_{i,j}}{r_{i+1} - r_i} + A_T \left(\frac{T_{i,j+1} - T_{i,j}}{\Delta z} + \frac{T_{i,j-1} - T_{i,j}}{\Delta z} \right) \right] \\ & + \frac{hA_{CV}}{\rho c V} (T_\infty - T_{i,j}) + \frac{Q_{fric}}{2\rho c V \pi} \end{aligned} \quad (C.12)$$

C.3 Equation for nodes on the wall on the outside of the cylinder

Start the derivation with the following heat balance.

$$\begin{aligned} \rho c V \frac{dT}{dt} = k A_I \frac{dT}{dr} \Big|_{i-1} + k A_T \frac{dT}{dz} \Big|_{j+1} + k A_B \frac{dT}{dz} \Big|_{j-1} \\ + h A_{CV} \Delta T + \frac{Q_{fric}}{2\pi} \end{aligned} \quad (C.13)$$

Where $Q_{fric} = 0$ if there is no friction. Integrating to find the volume and areas. The problem is axis-symmetric so all terms are divide by 2π .

$$V = \int_{z_i - \frac{\Delta z}{2}}^{z_i + \frac{\Delta z}{2}} \int_{\frac{r_i + r_{i-1}}{2}}^{r_i} r dr dz = \frac{\Delta z \left(4r_i^2 - (r_i + r_{i-1})^2 \right)}{8} \quad (C.14)$$

$$A_I = \int_{z_i - \frac{\Delta z}{2}}^{z_i + \frac{\Delta z}{2}} \left(\frac{r_i + r_{i-1}}{2} \right) dz = \frac{\Delta z (r_i + r_{i-1})}{2} \quad (C.15)$$

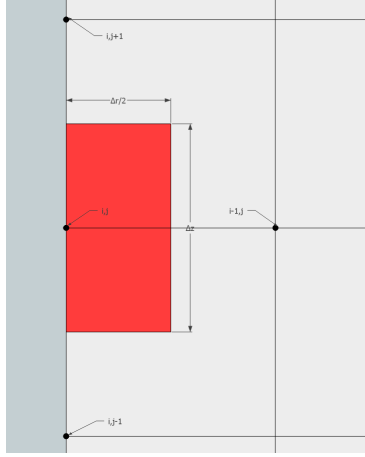


Figure C.3: Node on the wall on the outside of the cylinder

$$A_T = A_B = \int_{\frac{r_i+r_{i-1}}{2}}^{r_i} r dr = \frac{4r_i^2 - (r_i + r_{i-1})^2}{8} \quad (\text{C.16})$$

$$A_{CV} = r_i \int_{z_i - \frac{\Delta z}{2}}^{z_i + \frac{\Delta z}{2}} dz = r_i \Delta z \quad (\text{C.17})$$

Solving for $\frac{dT}{dt}$ and replacing the derivatives with forward and backward differences.

$$\begin{aligned} \frac{dT}{dt} = \frac{\alpha}{V} \left[A_I \frac{T_{i-1,j} - T_{i,j}}{r_i - r_{i-1}} + A_T \left(\frac{T_{i,j+1} - T_{i,j}}{\Delta z} + \frac{T_{i,j-1} - T_{i,j}}{\Delta z} \right) \right] \\ + \frac{hA_{Cv}}{\rho cV} (T_\infty - T_{i,j}) + \frac{Q_{fric}}{2\pi\rho cV} \end{aligned} \quad (\text{C.18})$$

C.4 Equation for nodes on the bottom/top of the cylinder

Start the derivation with the following heat balance.

$$\rho cV \frac{dT}{dt} = kA_O \left. \frac{dT}{dr} \right|_{i+1} + kA_I \left. \frac{dT}{dr} \right|_{i-1} + kA_T \left. \frac{dT}{dz} \right|_{j+1} + hA_{CH} \Delta T \quad (\text{C.19})$$

Integrating to find the volume and areas. The problem is axis-symmetric so all

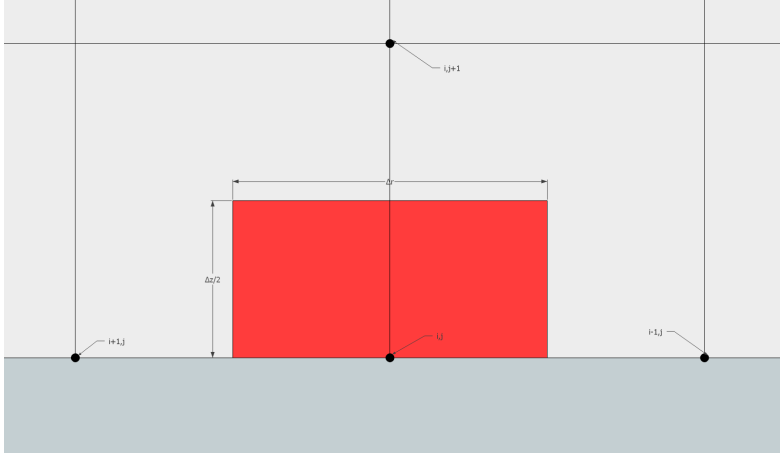


Figure C.4: Node on the bottom/top of the cylinder

terms are divide by 2π .

$$\begin{aligned}
 V &= \int_{z_i}^{z_i + \frac{\Delta z}{2}} \int_{\frac{r_i + r_{i-1}}{2}}^{\frac{r_{i+1} + r_i}{2}} r dr dz \\
 &= \frac{\Delta z \left((r_{i+1} + r_i)^2 - (r_i + r_{i-1})^2 \right)}{16}
 \end{aligned} \tag{C.20}$$

$$A_O = \int_{z_i}^{z_i + \frac{\Delta z}{2}} \left(\frac{r_{i+1} + r_i}{2} \right) dz = \frac{\Delta z (r_{i+1} + r_i)}{4} \tag{C.21}$$

$$A_I = \int_{z_i}^{z_i + \frac{\Delta z}{2}} \left(\frac{r_i + r_{i-1}}{2} \right) dz = \frac{\Delta z (r_i + r_{i-1})}{4} \tag{C.22}$$

$$A_T = A_{CH} = \int_{\frac{r_i + r_{i-1}}{2}}^{\frac{r_{i+1} + r_i}{2}} r dr = \frac{(r_{i+1} + r_i)^2 - (r_i + r_{i-1})^2}{8} \tag{C.23}$$

Solving for $\frac{dT}{dt}$ and replacing the derivatives with forward and backward differences.

$$\begin{aligned}
 \frac{dT}{dt} &= \frac{\alpha}{V} \left[A_O \frac{T_{i+1,j} - T_{i,j}}{r_{i+1} - r_i} + A_I \frac{T_{i-1,j} - T_{i,j}}{r_i - r_{i-1}} + A_T \frac{T_{i,j+1} - T_{i,j}}{\Delta z} \right] \\
 &+ \frac{h A_{CV}}{\rho c V} (T_\infty - T_{i,j})
 \end{aligned} \tag{C.24}$$

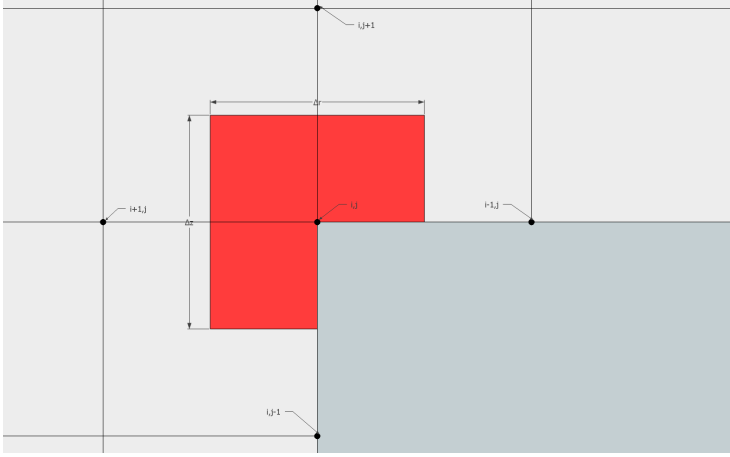


Figure C.5: Node at an internal corner on the inside of the cylinder

C.5 Equation for internal corner on the inside of the cylinder

Start the derivation with the following heat balance.

$$\rho c V \frac{dT}{dt} = k A_O \left. \frac{dT}{dr} \right|_{i+1} + k A_I \left. \frac{dT}{dr} \right|_{i-1} + k A_T \left. \frac{dT}{dz} \right|_{j+1} + k A_B \left. \frac{dT}{dz} \right|_{j-1} + h A_{CV} \Delta T + h A_{CH} \Delta T \quad (\text{C.25})$$

Integrating to find the volume and areas. The problem is axis-symmetric so all terms are divide by 2π .

$$\begin{aligned} V &= \int_{z_i}^{z_i + \frac{\Delta z}{2}} \int_{\frac{r_i - r_{i-1}}{2}}^{\frac{r_{i+1} + r_i}{2}} r dr dz + \int_{z_i - \frac{\Delta z}{2}}^{z_i} \int_{r_i}^{\frac{r_{i+1} + r_i}{2}} r dr dz \\ &= \frac{\Delta z}{16} [2(r_{i+1} + r_i)^2 - (r_i + r_{i-1})^2 - 4r_i^2] \end{aligned} \quad (\text{C.26})$$

$$A_O = \int_{z_i - \frac{\Delta z}{2}}^{z_i + \frac{\Delta z}{2}} \left(\frac{r_{i+1} + r_i}{2} \right) dz = \frac{\Delta z}{2} (r_{i+1} + r_i) \quad (\text{C.27})$$

$$A_I = \int_{z_i}^{z_i + \frac{\Delta z}{2}} \left(\frac{r_i + r_{i-1}}{2} \right) dz = \frac{\Delta z}{4} (r_i + r_{i-1}) \quad (\text{C.28})$$

$$A_T = \int_{\frac{r_i - r_{i-1}}{2}}^{\frac{r_{i+1} + r_i}{2}} r dr = \frac{(r_{i+1} + r_i)^2 - (r_i + r_{i-1})^2}{8} \quad (\text{C.29})$$

$$A_B = \int_{r_i}^{\frac{r_{i+1}+r_i}{2}} r dr = \frac{(r_{i+1} + r_i)^2 - 4r_i^2}{8} \quad (\text{C.30})$$

$$A_{CV} = r_i \int_{z_i - \frac{\Delta z}{2}}^{z_i} dz = \frac{r_i \Delta z}{2} \quad (\text{C.31})$$

$$A_{CH} = \int_{\frac{r_i - r_{i-1}}{2}}^{r_i} r dr = \frac{4r_i^2 - (r_i + r_{i-1})^2}{8} \quad (\text{C.32})$$

Solve for $\frac{dT}{dt}$ and replace the derivatives with forward or backward differences.

$$\begin{aligned} \frac{dT}{dt} = \frac{\alpha}{V} \left[A_O \frac{T_{i+1,j} - T_{i,j}}{r_{i+1} - r_i} + A_I \frac{T_{i-1,j} - T_{i,j}}{r_i - r_{i-1}} + A_T \frac{T_{i,j+1} - T_{i,j}}{\Delta z} \right. \\ \left. + A_B \frac{T_{i,j-1} - T_{i,j}}{\Delta z} \right] + \frac{h(T_\infty - T_{i,j})}{\rho c V} (A_{CV} + A_{CH}) \end{aligned} \quad (\text{C.33})$$

C.6 Equation for internal corner on the outside of the cylinder

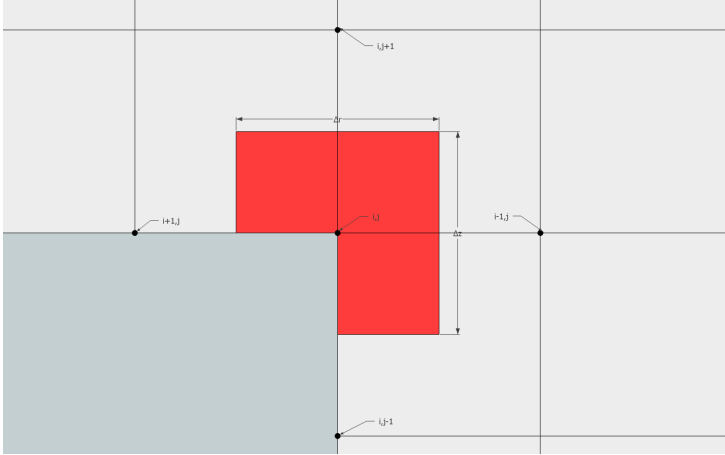


Figure C.6: Node at an internal corner on the outside of the cylinder

Start the derivation with the following heat balance.

$$\begin{aligned} \rho c V \frac{dT}{dt} = k A_O \left. \frac{dT}{dr} \right|_{i+1} + k A_I \left. \frac{dT}{dr} \right|_{i-1} + k A_T \left. \frac{dT}{dz} \right|_{j+1} + k A_B \left. \frac{dT}{dz} \right|_{j-1} \\ + h A_{CV} \Delta T + h A_{CH} \Delta T \end{aligned} \quad (\text{C.34})$$

Integrating to find the volume and areas. The problem is axis-symmetric so all terms are divide by 2π .

$$V = \int_{z_i}^{z_i + \frac{\Delta z}{2}} \int_{\frac{r_i - r_{i-1}}{2}}^{\frac{r_{i+1} + r_i}{2}} r dr dz + \int_{z_i - \frac{\Delta z}{2}}^{z_i} \int_{\frac{r_i - r_{i-1}}{2}}^{r_i} r dr dz \quad (C.35)$$

$$= \frac{\Delta z}{16} [(r_{i+1} + r_i)^2 - 2(r_i + r_{i-1})^2 + 4r_i^2]$$

$$A_O = \int_{z_i}^{z_i + \frac{\Delta z}{2}} \left(\frac{r_{i+1} + r_i}{2} \right) dz = \frac{\Delta z}{4} (r_{i+1} + r_i) \quad (C.36)$$

$$A_I = \int_{z_i - \frac{\Delta z}{2}}^{z_i} \left(\frac{r_i + r_{i-1}}{2} \right) dz = \frac{\Delta z}{2} (r_i + r_{i-1}) \quad (C.37)$$

$$A_T = \int_{\frac{r_i + r_{i-1}}{2}}^{\frac{r_{i+1} + r_i}{2}} r dr = \frac{(r_{i+1} + r_i)^2 - (r_i + r_{i-1})^2}{8} \quad (C.38)$$

$$A_B = \int_{\frac{r_i + r_{i-1}}{2}}^{r_i} r dr = \frac{4r_i^2 - (r_i + r_{i-1})^2}{8} \quad (C.39)$$

$$A_{CV} = r_i \int_{z_i - \frac{\Delta z}{2}}^{z_i} dz = \frac{r_i \Delta z}{2} \quad (C.40)$$

$$A_{CH} = \int_{r_i}^{\frac{r_{i+1} + r_i}{2}} r dr = \frac{(r_{i+1} + r_i)^2 - 4r_i^2}{8} \quad (C.41)$$

Solve for $\frac{dT}{dt}$ and replace the derivatives with forward and backward differences.

$$\frac{dT}{dt} = \frac{\alpha}{V} \left[A_O \frac{T_{i+1,j} - T_{i,j}}{r_{i+1} - r_i} + A_I \frac{T_{i-1,j} - T_{i,j}}{r_i - r_{i-1}} + A_T \frac{T_{i,j+1} - T_{i,j}}{\Delta z} \right. \\ \left. + A_B \frac{T_{i,j-1} - T_{i,j}}{\Delta z} \right] + \frac{h(T_\infty - T_{i,j})}{\rho c V} (A_{CV} + A_{CH}) \quad (C.42)$$

C.7 Equation for external corner on the inside of the cylinder

Start the derivation with the following heat balance.

$$\rho c V \frac{dT}{dt} = k A_O \frac{dT}{dr} \Big|_{i+1} + k A_T \frac{dT}{dz} \Big|_{j+1} + h A_{CV} \Delta T + h A_{CH} \Delta T \quad (C.43)$$

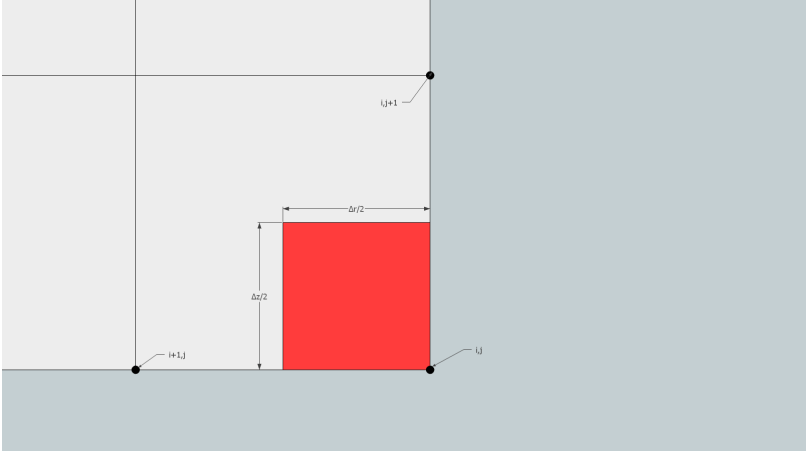


Figure C.7: Node at an external corner on the inside of the cylinder

Integrating to find the volume and areas. The problem is axis-symmetric so all terms are divide by 2π .

$$V = \int_{z_i}^{z_i + \frac{\Delta z}{2}} \int_{r_i}^{\frac{r_{i+1} + r_i}{2}} r dr dz = \frac{\Delta z ((r_{i+1} + r_i)^2 - 4r_i^2)}{16} \quad (\text{C.44})$$

$$A_O = \int_{z_i}^{z_i + \frac{\Delta z}{2}} \left(\frac{r_{i+1} + r_i}{2} \right) dz = \frac{\Delta z (r_{i+1} + r_i)}{4} \quad (\text{C.45})$$

$$A_T = A_{CH} = \int_{r_i}^{\frac{r_{i+1} + r_i}{2}} r dr = \frac{(r_{i+1} + r_i)^2 - 4r_i^2}{8} \quad (\text{C.46})$$

$$A_{CV} = r_i \int_{z_i}^{z_i + \frac{\Delta z}{2}} dz = \frac{r_i \Delta z}{2} \quad (\text{C.47})$$

Solve for $\frac{dT}{dt}$ and replace the derivatives with forward and backward differences.

$$\begin{aligned} \frac{dT}{dt} = \frac{\alpha}{V} & \left[A_O \frac{T_{i+1,j} - T_{i,j}}{r_{i+1} - r_i} + A_T \frac{T_{i,j+1} - T_{i,j}}{\Delta z} \right] \\ & + \frac{h(T_\infty - T_{i,j})}{\rho c V} (A_{CH} + h A_{CV}) \end{aligned} \quad (\text{C.48})$$

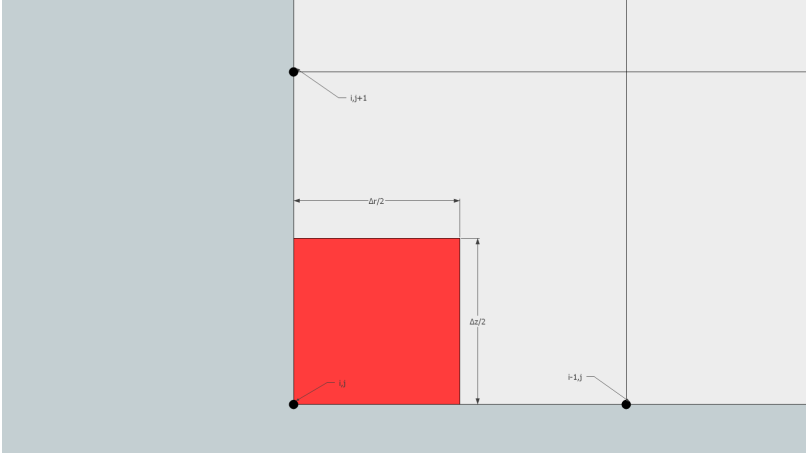


Figure C.8: Node at an external corner on the outside of the cylinder

C.8 Equation for external corner on the outside of the cylinder

Start the derivation with the following heat balance.

$$\rho c V \frac{dT}{dt} = k A_I \left. \frac{dT}{dr} \right|_{i-1} + k A_T \left. \frac{dT}{dz} \right|_{j+1} + h A_{CV} \Delta T + h A_{CH} \Delta T \quad (\text{C.49})$$

Integrating to find the volume and areas. The problem is axis-symmetric so all terms are divide by 2π .

$$V = \int_{z_i}^{z_i + \frac{\Delta z}{2}} \int_{\frac{r_i - r_{i-1}}{2}}^{r_i} r dr dz = \frac{\Delta z (4r_i^2 - (r_i + r_{i-1})^2)}{16} \quad (\text{C.50})$$

$$A_I = \int_{z_i}^{z_i + \frac{\Delta z}{2}} \left(\frac{r_i - r_{i-1}}{2} \right) dz = \frac{\Delta z (r_i + r_{i-1})}{4} \quad (\text{C.51})$$

$$A_T = A_{CH} = \int_{\frac{r_i - r_{i-1}}{2}}^{r_i} r dr = \frac{4r_i^2 - (r_i + r_{i-1})^2}{8} \quad (\text{C.52})$$

$$A_{CV} = r_i \int_{z_i}^{z_i + \frac{\Delta z}{2}} dz = \frac{r_i \Delta z}{2} \quad (\text{C.53})$$

Solve for $\frac{dT}{dt}$ and replace the derivatives with forward and backward differences.

$$\begin{aligned} \frac{dT}{dt} = \frac{\alpha}{V} & \left[A_I \frac{T_{i-1,j} - T_{i,j}}{r_i - r_{i-1}} + A_T \frac{T_{i,j+1} - T_{i,j}}{\Delta z} \right] \\ & + \frac{h(T_\infty - T_{i,j})}{\rho c V} (A_{CV} + A_{CV}) \end{aligned} \quad (\text{C.54})$$

Appendix D

The program

A program has been written to solve the transient behavior of the system. To allow users that are not familiar with the code to use the program a Graphical User Interface(GUI) has been developed.

By running the file GUI.m in MATLAB the GUI shown in figure D.1 will pop up.

1. In the «Variables» panel one can enter the desired piston amplitude, piston frequency, ambient heat transfer coefficient and the inside heat transfer coefficient.
2. In the «Initial values» panel one can enter the initial values for the simulation. That includes the initial pressure, temperature and the start and stop time.
3. The «Simulation» panel contains buttons to run the simulation.
 - (a) By pressing the «Start» button the simulation starts with the input/initial values specified in 1-2. A Progress bar will pop up and show how many percent of the simulation that is completed.
 - (b) By pressing the «Cancel» button on the progress bar the simulation is stopped.
 - (c) By pressing «Resume» the simulation resumes from the point where the simulation was stopped, or from the endpoint of variables loaded in to the program.
 - (d) By pressing «Resume from endpoint» the old variables are deleted and the simulation resumes from the endpoint. This may be used to avoid running out of memory. If the previous values are of interest it is recommended to save them before pressing this button.
 - (e) By pressing «Load variables» a pop up menu to load variables from a earlier simulation appears.

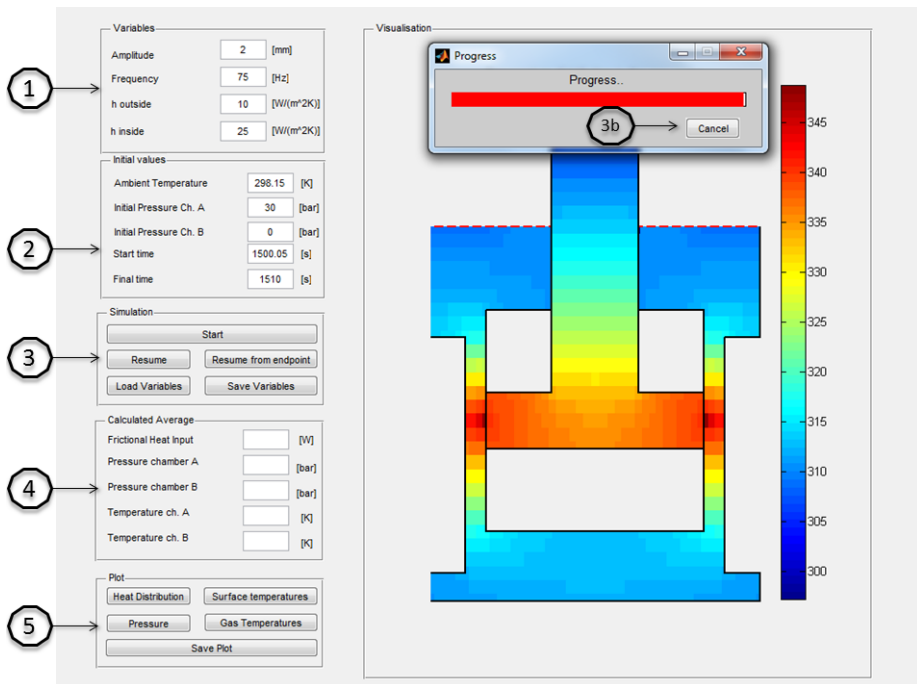


Figure D.1: The graphical user interface.

- (f) By pressing «Save variables» a pop up menu to save variables from a simulation appears.
4. The «Calculated Average» panel shows the calculated average values of the frictional heat input and the pressures and temperatures in chamber A and B.
 5. The «Plot» panel contains buttons to plot heat distribution, density, pressure and gas temperatures. When one of the buttons is pressed the plot will appear in the «Visualization» panel. By pressing «Save Plot» a pop up menu to save the plot appears. It is possible to plot during a simulation.

Appendix E

Simulations and tests

The following simulations have been performed. In addition many simulations were carried out while programming to make sure the physics seemed right. Simulations that showed erroneous answers due to errors in the programming (signs etc.) is not included.

Table E.1: Simulations performed and test results received.

Amplitude [<i>mm</i>]	Initial Pressure [<i>bar</i>]	Frequency [<i>Hz</i>]	Configuration	Comments
16	300	100	Rod and piston seal installed, both chambers pressurized, no heat transfer through lubrication oil.	The simulations showed extremely high temperatures. It seemed unreasonable with no heat transfer between cylinder/piston, therefore it was decided to implement it.
16	300	100	Rod and piston seal installed, both chambers pressurized, heat transfer through lubrication oil.	The heat transfer between piston/cylinder seemed more realistic. The simulation still showed extremely high temperatures. The input was design criteria, it was decided to use input values similar to the tests run by Resonator.

Table E.1: Simulations performed and test results received.

Amplitude [<i>mm</i>]	Initial Pressure [<i>bar</i>]	Frequency [<i>Hz</i>]	Configuration	Comments
5	25	70	Rod and piston seal installed, both chambers pressurized, heat transfer through lubrication oil.	The simulations still showed very high temperatures compared to what Resonator said they experienced. It was decided that I should visit Resonators workshop to have a look at the device. The visit showed that the configuration was different than what was stated earlier.
2	30	75	Only piston seal installed, chamber A pressurized, heat transfer through lubrication oil.	Test results received. Figures 4.2 and 4.3.
2	30	75	Only piston seal installed, chamber A pressurized, heat transfer through lubrication oil.	The simulation showed a different slope than the test results. It was decided to change the boundary conditions on the top and bottom surface of the gas spring. Figure 4.1.
2	30	75	Only piston seal installed, chamber A pressurized, heat transfer through lubrication oil.	The simulation showed similar slope as the test results but the temperature was too high. It was decided to adjust the friction levels. Figure 4.4.

Table E.1: Simulations performed and test results received.

Amplitude [<i>mm</i>]	Initial Pressure [<i>bar</i>]	Frequency [<i>Hz</i>]	Configuration	Comments
2	30	75	Only piston seal installed, chamber A pressurized, heat transfer through lubrication oil, adjusted friction levels.	The simulation showed good agreement with the test results. Figures 4.5 and 4.6.
3.5	51	94	Only piston seal installed, chamber A pressurized, heat transfer through lubrication oil.	Test results received. Figure 4.11.
3.5	51	94	Only piston seal installed, chamber A pressurized, heat transfer through lubrication oil, adjusted friction levels.	The comparison of the test and the simulation showed that further work needs to be carried out to improve the friction model. Figure 4.11.
-	-	104	Only piston seal installed, chamber A pressurized, heat transfer through lubrication oil.	Test results received. No time available to process the data.